A Meshless Method Based on the Moving Least Squares Approach for Approximate Solution of the Generalized 2-D Nonlinear Benjamin–Bona–Mahony–Burgers Equation

Said Elbostani and Rachid El Jid

Abstract—In this work, we numerically solve the 2D nonlinear generalized Benjamin-Bona-Mahony-Burgers (BBMB) equation by using the moving least squares (MLS) method. This approach is explained and used to formulate the generalized BBMB equation. The finite difference method approximates the time derivative. Stability conditions and convergence analysis are provided for the time semi-discrete formulation. The correctness and effectiveness of the proposed approach are proven with various problems. Furthermore, the MLS method is compared to several methods in the literature through different examples to ensure its applicability and effectiveness. The presented method gave high accuracy and convergence results compared to other methods used to solve this problem.

Index Terms—Generalized Benjamin–Bona–Mahony–Burgers (BBMB) equation, Moving least squares (MLS), Meshless method, Stability analysis.

I. Introduction

In the larger field of sciences and engineering, several problems are modulated by Nonlinear Partial Differential Equations (NPDEs) [49], [17]. The smooth functioning of various engineering disciplines [4], [11] as well as phenomena in physics such as liquid-gas bubble interactions [57] and mathematical physics contexts [20] can be comprehensively studied through the solution of these equations. Nonlinear PDEs are considerably more complicated than linear PDEs, and as a result, finding an exact solution is usually limited to simpler situations or certain types of equations. In such cases, numerical solutions may effectively solve these difficulties.

We employ in this study the MLS approach to numerically approximate the generalized two-dimensional nonlinear BBMB equation. [18], [19], [31].

$$\begin{cases} \dfrac{\partial u}{\partial t} - \dfrac{\partial \Delta u}{\partial t} - \Delta u + \nabla \cdot u = \nabla \cdot G(u) + g(x,y,t), \\ (x,y) \in \Omega \subset \mathbb{R}^2, \quad t \in (0,T]. \end{cases} \tag{1}$$

The conditions related to the problem are as follows:

$$\begin{cases} u(x,y,t) &= \phi(t), \;\; (x,y) \in \partial\Omega, \\ u(x,y,0) &= u_0(x,y), \quad (x,y) \in \Omega, \end{cases} \tag{2}$$

where u_0, ϕ and g are predefined smooth functions, G represents the nonlinear term in the equation, and Δ and ∇ are the classical operators in differential calculus.

The BBMB equation (1) is commonly employed in the analysis of various wave phenomena in different physical contexts, such as the study of long-wavelength surface waves in liquids [5], [45]. The one-way movement of small amplitude long waves on water is modeled by the Benjamin–Bona–Mahony equation [14]. Fluid acoustic-gravity waves and a-harmonic crystal acoustic waves were studied in [50]. Abbasbandy et al. [1] investigated hydromagnetic waves in cold plasma and acoustic-gravity waves in compressible fluids in their study. In nonlinear dispersive systems, the BBMB problem is crucial for understanding the unidirectional propagation of long waves [40]. in nonlinear dispersive media [9], [37], [34] and traffic flow modeling [41].

The first step after modeling an equation involves studying the theoretical analysis of the uniqueness and existence of the solution. If the existence of solutions is confirmed, we proceed to their determination using appropriate analytical methods to analyze and explain the phenomena.

The BBMB equation (1) have been solved using various analyzes by several authors. For multidimensional generalized BBM-Burgers equations, Zhao et al. [56] studied global smooth solutions, focusing on their existence and convergence. The existence of a global attractor was established by Wang et al. in [53]. Analytic solutions for the highly nonlinear type of BBMB equations were obtained in [16], [35], [12]. Furthermore, many scientists have proposed various analytical methods to solve these types of equations. Other methods used to obtain analytical solutions for the BBMB equation include those described in [3], [2], and [28], as well as the Optimal Homotopy Asymptotic Method (OHAM) [10]. A novel analytical method called the Exp-Function method was introduced and applied for solving a specific form of the generalized nonlinear BBMB equation [25], [33]. A nonlinear differential equation was solved using the Kudryashov approach in [15] to find its exact solution.

Additionally, a certain class of problems has difficulties in finding exact solutions (1), Numerical methods have become valuable tools for determining solutions to such equations. Methods like the Finite Difference Method (FDM) were studied. The BBMB equation was numerically solved using a sixth-order finite difference

Manuscript received December 28, 2023; revised July 1, 2024.

S. Elbostani is Doctoral Student in Department of Mathematics and Computing Sciences, Faculty of Sciences and Technology, University Hassan I, Settat, Morocco. (corresponding author; e-mail: elboustanisaid10@gmail.com)

R. El Jid is Professor in Department of Mathematics and Computing Sciences, Faculty of Sciences and Technology, University Hassan I, Settat, Morocco. (e-mail:rachideljid@gmail.com)

scheme in [39]. Zhang et al. [55] introduced linearized finite difference schemes for their research, and the Finite Element Method (FEM) was used by Kadri et al. and other researchers [32], [54].

In fact, these approaches often face challenges with complex meshing, which is a notable drawback. To overcome these limitations, meshless methods offer unique simplicity while achieving solution accuracy comparable to these methods. Various types of meshless methods are available, including the Spectral Meshless Radial Point Interpolation (SMRPI) method utilized by Shivanian et al. [48], and the Legendre Spectral Element Method (LSEM) employed by Dehghan et al. [19]. The Singular Boundary Method (SBM) was utilized by Aslefallah et al. [7]. Haq et al. [27] utilized the Haar wavelets method in their work. Cubic B-spline basis functions were utilized by Majeed et al. [42]. The Quintic Hermite Collocation Method (QHCM) was employed by Arora et al. [6]. Kukrej et al. [36] utilized the b-spline collocation method. The generalized 2-D nonlinear BBMB equation was solved using the Modified Cubic B-spline Differential Quadrature (MCBSDQ) method [31].

The main advantages of meshless techniques is their ability to provide accurate solutions for specific equation classes without the necessity of mesh connectivity. Unlike traditional methods, meshless approaches do not require subdomain connectivity, surface discretization, or normal vectors of the surface subdomain. The methods that have been developed for solving the BBMB equation often encounter challenges such as ill-conditioned systems or complex formulations that lead to instability or difficulty in implementation. Moreover, many of these methods require constructing approximation shape functions and handling complex integration procedures.

In this paper, we apply a different meshless technique, known as the MLS method to solve the problem proven in the equation (1). The MLS method, initially introduced by Shepard [46] and subsequently refined by various researchers, has found applications in constructing surfaces and interpolating scattered data [23]. Various classes of PDEs have been solved using the MLS method, which has gained significant popularity for approximating solutions [22], [43], [38] and for fractional partial differential equations in high-dimensional spaces [26], [30], [29]. This method has been increasingly adopted in recent years due to its effectiveness in providing accurate solutions to complex mathematical problems involving multiple dimensions [47], [52], [21].

The objective of this research is to validate the effectiveness of the MLS method compared to other meshless methods for solving the equation (1). The literature includes various meshless methods for approximating solutions to this type of equation. the application of the MLS method specifically to this equation (1) has not been explored. This lack of application motivated the present investigation.

The outline for this study is arranged as: The initial Section I provides an introduction to the problem (1). Section II presented the current method. The description of the MLS is applied to the BBMB equation in Section III. Section IV discussed the numerical analysis of the presented approach. The accuracy and effectiveness of the suggested technique are analyzed by solving several problems in Section V. Finally, VI contains the conclusion.

II. The MLS approximation

Given that $u_j = u(\mathbf{x}_j)$, where $\mathbf{x}_j,\ j = 1, ..., M$ denotes nodes in the domain Ω. An approximation function for $u(\mathbf{x})$ using the MLS method is given as:

$$u^h(\mathbf{x}) = \sum_{i=1}^{m} p_i(\mathbf{x})\lambda_i(\mathbf{x}) = \mathbf{p}^T(\mathbf{x})\lambda(\mathbf{x}), \tag{3}$$

where $\lambda(\mathbf{x}) = [\lambda_1(\mathbf{x}), ..., \lambda_m(\mathbf{x})]$ is an unknown column vector containing variable functions. $\mathbf{p}^T(\mathbf{x}) = [p_1(\mathbf{x})\quad p_2(\mathbf{x})\ \dots\ p_m(\mathbf{x})]$ is a complete monomials basis of order m.

We need to minimize the weighted discrete L_2 norm to determine the coefficient $\lambda(\mathbf{x})$:

$$\begin{aligned}\mathbb{J}_{\mathbf{x}}(\lambda) &= \sum_{j=1}^{M} w_j(\mathbf{x}) \left(u^h(\mathbf{x}_j, \mathbf{x}) - u_j\right)^2 \\ &= \sum_{j=1}^{M} w_j(\mathbf{x}) \left(\mathbf{p}^T(\mathbf{x}_j)\lambda(\mathbf{x}) - u_j\right)^2,\end{aligned} \tag{4}$$

where $\{\mathbf{x}_j,\ j = 1, ..., M\}$ are the points in the neighborhood of nodal point $\mathbf{x}$, $w_j(\mathbf{x})$ is a nonnegative function with compact support and is called a weight function. The functional $\mathbb{J}_{\mathbf{x}}$ is a nonnegative summation. Thus, the coefficients $\lambda(\mathbf{x})$ can be obtained using this condition $\frac{\partial \mathbb{J}_{\mathbf{x}}}{\partial \lambda} = 0$.

Hence, the partial derivatives of $\mathbb{J}_{\mathbf{x}}$ are given as:

$$\begin{aligned}\frac{\partial \mathbb{J}_{\mathbf{x}}}{\partial \lambda_i} &= 2\sum_{j=1}^{M} w_j(\mathbf{x})p_i(\mathbf{x}_j)\left[\mathbf{p}^T(\mathbf{x}_j)\lambda(\mathbf{x}) - u_j\right] \\ &= 2\left[\sum_{j=1}^{M} w_j(\mathbf{x})p_i(\mathbf{x}_j)\mathbf{p}^T(\mathbf{x}_j)\lambda(\mathbf{x}) - w_j(\mathbf{x})p_i(\mathbf{x}_j)u_j\right].\end{aligned}$$

for all $i = 1, ..., m$.

After arrangement, the above condition of $\mathbb{J}_{\mathbf{x}}$ can be written as:

$$\sum_{j=1}^{M} w_j(\mathbf{x})\mathbf{p}(\mathbf{x}_j)\mathbf{p}^T(\mathbf{x}_j)\lambda(\mathbf{x}) = \sum_{j=1}^{M} w_j(\mathbf{x})\mathbf{p}(\mathbf{x}_j)u_j. \tag{5}$$

Rewriting the equation (5) in this form:

$$\mathbf{A}(\mathbf{x})\lambda(\mathbf{x}) = \mathbf{B}(\mathbf{x})\mathbf{u}, \tag{6}$$

where the column vector $\mathbf{u}$, the matrix $\mathbf{B}(\mathbf{x})$, and the matrix $\mathbf{A}(\mathbf{x})$ are chosen as follows:

$$\mathbf{u}^T = [u_1\quad u_2\quad \cdots\quad u_M], \tag{7}$$

$$\mathbf{A}(\mathbf{x}) = \sum_{j=1}^{M} w_j(\mathbf{x})\mathbf{p}(\mathbf{x}_j)\mathbf{p}^T(\mathbf{x}_j) \tag{8}$$

and

$$\mathbf{B}(\mathbf{x}) = [w_1(\mathbf{x})\mathbf{p}(\mathbf{x}_1)\ \ w_2(\mathbf{x})\mathbf{p}(\mathbf{x}_2)\ \ \cdots\ \ w_M(\mathbf{x})\mathbf{p}(\mathbf{x}_M)]. \tag{9}$$

We found the unknown $\lambda(\mathbf{x})$ using Eq. (6), therefore we can substitute this value into Eq. (3) to give the approximation $u^h(\mathbf{x})$ as:

$$u^h(\mathbf{x}) = \sum_{j=1}^{M} \psi_j(\mathbf{x}) u_j = \Psi^T(\mathbf{x}).\mathbf{u}, \tag{10}$$

where

$$\Psi^T(\mathbf{x}) = [\psi_1(\mathbf{x}) \dots \psi_M(\mathbf{x})] = \mathbf{p}^T(\mathbf{x})\mathbf{A}^{-1}(\mathbf{x})\mathbf{B}(\mathbf{x}), \tag{11}$$

or

$$\psi_j(\mathbf{x}) = \mathbf{p}^T(\mathbf{x})[\mathbf{A}(\mathbf{x})]^{-1} w_j(\mathbf{x})\mathbf{p}\left(\mathbf{x}_j\right). \tag{12}$$

$\psi_j(\mathbf{x})$ is named the shape function at the node $\mathbf{x}_j$ in this method. We need to construct shape functions and weighting functions w_j.

This paper employs three weight functions corresponding to the node j as follows:

The cubic weight function is:

$$w_j(\mathbf{x}) = \begin{cases} \frac{2}{3} - 4\left(\frac{d_j}{r}\right)^2 + 4\left(\frac{d_j}{r}\right)^3, \\ if\ 0 \le \frac{d_j}{r} \le \frac{1}{2}, \\ \frac{4}{3} - 4\left(\frac{d_j}{r}\right) + 4\left(\frac{d_j}{r}\right)^2 - \frac{4}{3}\left(\frac{d_j}{r}\right)^3, \\ if\ \frac{1}{2} < \frac{d_j}{r} \le 1, \\ 0\ if\ \frac{d_j}{r} > 1. \end{cases} \tag{13}$$

The quartic weight function is:

$$w_j(\mathbf{x}) = \begin{cases} 1 - 6\left(\frac{d_j}{r}\right)^2 + 8\left(\frac{d_j}{r}\right)^3 - 3\left(\frac{d_j}{r}\right)^4 \\ if\ 0 \le \frac{d_j}{r} \le 1, \\ 0\ if\ \frac{d_j}{r} > 1. \end{cases} \tag{14}$$

The Gaussian weight function (GWF) is usually expressed as:

$$w_j(\mathbf{x}) = \begin{cases} \frac{\exp\left[-\left(\frac{d_j}{\mu}\right)^2\right] - \exp\left[-\left(\frac{r}{\mu}\right)^2\right]}{1-\exp\left[-\left(\frac{r}{\mu}\right)^2\right]} & 0 \le \frac{d_j}{r} < 1, \\ 0 & \frac{d_j}{r} \ge 1. \end{cases} \tag{15}$$

where $d_j = \|\mathbf{x} - \mathbf{x}_j\|$, μ is a constant regulate for the GWF, and h is the radius of the support domain around the node $\mathbf{x}_j$. We employ the simplified form of the GWF:

$$w_j(\mathbf{x}) = \begin{cases} \frac{\exp(-s^2 r^2) - \exp(-s^2)}{1-\exp(-s^2)} & 0 \le r < 1, \\ 0 & r \ge 1. \end{cases} \tag{16}$$

where $s = \frac{r}{\mu}$ and $h = \frac{d_j}{r}$.

III. Description of the MLS method

First, we will apply the FDM to discretize the first time derivative, and for the other time derivatives of the problem (1), we will apply the generalized θ scheme. Second, we will discuss the spatial discretization technique used with the moving least squares method

$$\frac{\partial u^n}{\partial t} \approx \frac{u^{n+1} - u^n}{\Delta t}\ and\ \frac{\partial \Delta u^n}{\partial t} \approx \frac{\Delta u^{n+1} - \Delta u^n}{\Delta t}. \tag{17}$$

For the Laplace and gradient operators, we apply the θ-scheme. For $\theta = 1/2$, we obtain:

$$\Delta u \approx \frac{\Delta u^{n+1} + \Delta u^n}{2}, \quad \nabla.u \approx \frac{\nabla \cdot u^{n+1} + \nabla \cdot u^n}{2},$$
$$\text{and } g(x,y,t) \approx \frac{g^{n+1} + g^n}{2}. \tag{18}$$

For $\theta = 0$, the nonlinear term becomes:

$$\nabla \cdot G(u) \approx \nabla \cdot G\left(u^n\right), \tag{19}$$

where $u^n = u\left(x, y, t^n\right)$.

After replacing Eqs. (17), (18) and (19) in the Eq. (1), we get this equation:

$$\frac{u^{n+1} - u^n}{\Delta t} - \frac{\Delta u^{n+1} - \Delta u^n}{\Delta t} - \frac{\Delta u^{n+1} + \Delta u^n}{2} + \frac{\nabla \cdot u^{n+1} + \nabla \cdot u^n}{2} = \nabla \cdot G\left(u^n\right) + \frac{g^{n+1} + g^n}{2} + \mathcal{O}(\Delta t), \tag{20}$$

where u^n represents the exact solution at instant t^n. Neglecting the term $\mathcal{O}(\Delta t)$, we rewrite the Eq. (20) as follows for all $(x,y) \in \Omega$

$$\begin{aligned} &U^{n+1} - \left(1 + \frac{\Delta t}{2}\right)\Delta U^{n+1} + \frac{\Delta t}{2}\nabla \cdot U^{n+1} \\ &= U^n - \left(1 - \frac{\Delta t}{2}\right)\Delta U^n - \frac{\Delta t}{2}\nabla \cdot U^n + \Delta t \nabla \cdot G\left(U^n\right) \\ &+ \Delta t\left(\frac{g^{n+1} + g^n}{2}\right), \end{aligned} \tag{21}$$

where U^n is the approximate solution of the problem (1) at instant t^n and $n = 0, 1, \dots, N-1$.

Now, for space discretization, we discretize this domain Ω into M grid points as follows:
$x_i = (i-1)h_x$, $y_j = (j-1)h_y$ where $h_x = 1/(M_x - 1)$ is the step size of direction x, $h_y = 1/(M_y - 1)$ is the step size of direction y, and $M = M_x M_y$.

The approximation $U^n(x,y)$ at $n = 0, \dots, N-1$ is given by the MLS method as:

$$U^n\left(x, y\right) = \sum_{j=1}^{M} \lambda_j^n \psi_j\left(x, y\right),\ for\ (x,y) \in \Omega, \tag{22}$$

where $\psi_j(x,y)$, $j = 1, ..., M$ are defined in Eq (12) and λ^n is a vector containing unknown coefficients which must be obtained by solving a linear system.

Replacing M collocation points in Eq. (22), we get the following system:

$$U^n\left(x_i, y_i\right) = \sum_{j=1}^{M} \lambda_j^n \psi_j\left(x_i, y_i\right), \quad i = 1, ..., M. \tag{23}$$

Rewrite the Eq. (23) in matrix form:

$$\mathbf{U}^n = \mathbf{\Psi}\lambda^n, \quad n = 0, ..., N, \tag{24}$$

where

$$\mathbf{U}^n = \left[U_1^n, U_2^n, \dots, U_M^n\right]^T,$$
$$\lambda^n = \left[\lambda_1^n, \lambda_2^n, \dots, \lambda_M^n\right]^T$$

and $\mathbf{\Psi}$ is an $M \times M$ matrix given by:

$$\mathbf{\Psi} = [\psi_{ji}] = \begin{pmatrix} \psi_{11} & \cdots & \psi_{1M} \\ \vdots & \ddots & \vdots \\ \psi_{M1} & \cdots & \psi_{MM} \end{pmatrix}, \tag{25}$$

where $\psi_{ij} = \psi_j\,(x_i, y_i)$.

We have M_b boundary points in Eq. (1) and $M - M_b$ internal points. Consequently, the matrix $\mathbf{\Psi}$ is divided as: $\mathbf{\Psi} = \mathbf{T} + \mathbf{S}$ where

$$\mathbf{T} = [t_{ij}] = \begin{cases} 0, & i = 1, ..., M_b,\ j = 1, ..., M, \\ \mathbf{\Psi}_{ij}, & i = M_b + 1, ..., M,\ j = 1, ..., M, \end{cases}$$

$$\mathbf{S} = [s_{ij}] = \begin{cases} \mathbf{\Psi}_{ij}, & i = 1, ..., M_b,\ j = 1, ..., M, \\ 0, & i = M_b + 1, ..., M,\ j = 1, ..., M. \end{cases}$$

We discretize ΔU^n and $\nabla \cdot U^n$ using the Eq. (22) for $n = 1, ..., N$

$$\begin{aligned} \Delta U^n(x, y) &= \sum_{j=1}^{M} \lambda_j^n \Delta\psi_j(x, y), \\ \nabla \cdot U^n(x, y) &= \sum_{j=1}^{M} \lambda_j^n \nabla \cdot \psi_j(x, y), \end{aligned} \tag{26}$$

where $\Delta\psi_j(x, y)$ and $\nabla \cdot \psi_j(x, y)$ are obtained in [51], [24] and [8].

Substituting $M - M_b$ internal points into Eq. (26), we have:

$$\begin{aligned} \Delta U^n(x_i, y_i) &= \sum_{j=1}^{M} \lambda_j^n \Delta\psi_j(x_i, y_i), \\ \nabla \cdot U^n(x_i, y_i) &= \sum_{j=1}^{M} \lambda_j^n \nabla \cdot \psi_j(x_i, y_i), \end{aligned} \tag{27}$$

then Eq. (27) can be rewritten:

$$\Delta \mathbf{U}^n = \mathbf{D}\lambda^n \text{ and } \nabla \cdot \mathbf{U}^n = \mathbf{C}\lambda^n, \tag{28}$$

where

$$\begin{aligned} \nabla \cdot \mathbf{U}^n &= \left[\nabla \cdot U_1^n, \nabla \cdot U_2^n, \ldots, \nabla \cdot U_M^n\right]^T, \\ \Delta \mathbf{U}^n &= \left[\Delta U_1^n, \Delta U_2^n, \ldots, \Delta U_M^n\right]^T, \end{aligned}$$

the matrices $\mathbf{D}$ and $\mathbf{C}$ are $M \times M$ matrix given by:

$$\mathbf{D} = \begin{cases} 0, & i = 1, ..., M_b,\ j = 1, ..., M, \\ \Delta\psi_j(x_i, y_i), & i = M_b + 1, ..., M,\ j = 1, ..., M, \end{cases}$$

$$\mathbf{C} = \begin{cases} 0, & i = 1, ..., M_b,\ j = 1, ..., M, \\ \nabla \cdot \psi_j(x_i, y_i), & i = M_b + 1, ..., M,\ j = 1, ..., M. \end{cases}$$

By replacing the boundary conditions in Eq. (1) together with $M - M_b$ nodes in the domain in Eq. (21) and using Eqs. (28) and (24), we find this recursive relation:

$$\begin{aligned} &\left(\mathbf{\Psi} - \left(1 + \frac{\Delta t}{2}\right)\mathbf{D} + \frac{\Delta t}{2}\mathbf{C}\right)\lambda^{n+1} \\ &= \left(\mathbf{T} - \left(1 - \frac{\Delta t}{2}\right)\mathbf{D} - \frac{\Delta t}{2}\mathbf{C} + \Delta t\mathbf{G}^n\mathbf{C}\right)\lambda^n + \mathbf{H}^{n+1}, \end{aligned} \tag{29}$$

for $n = 0, 1, ..., N$.

Where $\mathbf{G}^n$ is a diagonal matrix defined by

$$\mathbf{G}^n = diag\left\{\begin{cases} 0, & i = 1, ..., M_b, \\ \frac{dG(U_i^n)}{du} & i = M_b + 1, ..., M, \end{cases}\right\}$$

and

$$\mathbf{H}^{n+1} = \begin{cases} \phi(t^{n+1}), & i = 1, ..., M_b, \\ \Delta t\left(\frac{g(x_i, y_i, t^{n+1}) + g(x_i, y_i, t^n)}{2}\right), & i = M_b + 1, ..., M, \end{cases}$$

Eq. (29) can be simplified for $n = 0, 1, ..., N - 1$ as:

$$\mathbf{L}\lambda^{n+1} = \mathbf{B}\lambda^n + \mathbf{H}^{n+1}, \tag{30}$$

where

$$\mathbf{L} = \mathbf{\Psi} - \left(1 + \frac{\Delta t}{2}\right)\mathbf{D} + \frac{\Delta t}{2}\mathbf{C},$$

$$\text{and} \qquad \mathbf{B} = \mathbf{T} - \left(1 - \frac{\Delta t}{2}\right)\mathbf{D} - \frac{\Delta t}{2}\mathbf{C} + \Delta t\mathbf{G}^n\mathbf{C}.$$

IV. Stability analysis of the presented method

We analyze the semi-discrete equation (21) to study the convergence and stability conditions.

Firstly, we consider the following functional spaces [13]:

$$\begin{aligned} H^1(\Omega) &= \left\{v \in L^2(\Omega), \nabla \cdot v \in L^2(\Omega)\right\}, \\ \text{and} \qquad H_0^1(\Omega) &= \left\{v \in H^1(\Omega), v|_{\partial\Omega} = 0\right\}, \end{aligned}$$

where

$$L^2(\Omega) = \left\{v : \int_\Omega |v|^2 d\Omega < \infty\right\},$$

The classical inner products of the above spaces are chosen as:

$$\langle v, w\rangle_{L^2(\Omega)} = \int_\Omega vw d\Omega, \quad \langle v, w\rangle_{H^1(\Omega)} = \langle v, w\rangle + \langle \nabla v, \nabla w\rangle.$$

The norms in $H^1(\Omega)$ and $L^2(\Omega)$ are defined as

$$\begin{aligned} \|v\|_{H^1(\Omega)} &= \sqrt{\|v\|_{L^2(\Omega)}^2 + \|\nabla v\|_{L^2(\Omega)}^2}, \\ \|v\|_{L^2(\Omega)} &= \sqrt{\langle v, v\rangle}. \end{aligned}$$

Now, we use the analysis obtained by Dehghan et al. [19] in this section.

Theorem 1. ([19]) Let $U^n \in H_0^1(\Omega)$. By considering $\Delta t \le \dfrac{1}{\frac{5}{2} + \mathcal{L}}$, semi-discrete scheme given in Eq. (21) will be stable in H^1-norm, where $\mathcal{L}$ is the constant of Lipschitz condition of G.

Theorem 2. ([19]) Suppose that u^n, U^n belong to $H_0^1(\Omega)$ and denote solutions of Equations (20) and (21), respectively. Then, the convergence order of time-discrete scheme (21) is $\mathcal{O}(\delta t)$.

Rewrite Eq. (30) as follows:

$$\lambda^{n+1} = \mathbf{L}^{-1}\mathbf{B}\lambda^n + \Delta t\mathbf{L}^{-1}\mathbf{H}^{n+1}, \tag{31}$$

Multiplying Eq. (31) by the matrix $\mathbf{\Psi}$, we get for $n = 0, 1, ..., N - 1$,

$$\mathbf{U}^{n+1} = \mathbf{\Psi}\mathbf{L}^{-1}\mathbf{B}\mathbf{\Psi}^{-1}\mathbf{U}^n + \Delta t\mathbf{\Psi}\mathbf{L}^{-1}\mathbf{H}^{n+1}. \tag{32}$$

Let U^n_{exact} and U^n denote the exact and numerical solutions at $n\Delta t$ of Eq. (29). We defined the convergence error at $n\Delta t$ by: $\mathcal{E}^n = U^n_{exact} - U^n$.

Now, subtracting the equations of exact and numerical solutions, we obtain

$$\mathcal{E}^{n+1} = \mathbf{W}\mathcal{E}^n,$$

where $\mathbf{W} = \mathbf{\Psi}\mathbf{L}^{-1}\mathbf{B}\mathbf{\Psi}^{-1}$ and the vector $\mathbf{H}^{n+1}$ contains known functions g and ϕ.

Hence, the stability condition of this presented method is written as [44]

$$\lambda_{sr} = \max_{1\leq i\leq M} (|\lambda_i(\mathbf{W})|) < 1, \tag{33}$$

where λ_{sr} is the largest eigenvalue of the matrix $\mathbf{W}$ and is also called the spectral radius of convergence.

V. Result analysis

We give the results analysis of the current technique by solving various problems. Firstly, we compared the proposed method with two problems obtained in [18], [19] and [31].

Secondly, to provide the exactness and efficiency of the method, we consider two additional problems.

We evaluate the convergence and precision of the suggested approach in this study by implementing the described procedure with Δt and varying values of M.

The simulations of the examples used three error norms as:

$$L_\infty = \max_{1\leq j\leq M} \left|u\left(\mathbf{x}_j, T\right) - U\left(\mathbf{x}_j, T\right)\right|,$$

$$L_2 = \sqrt{\sum_{j=1}^{M} \left|u\left(\mathbf{x}_j, T\right) - U\left(\mathbf{x}_j, T\right)\right|^2},$$

$$\text{and} \quad \text{RMS} = \sqrt{\frac{1}{M}\sum_{j=1}^{M} \left|u\left(\mathbf{x}_j, T\right) - U\left(\mathbf{x}_j, T\right)\right|^2}.$$

and the following basis is chosen to construct the shape functions:

$$\mathbf{p}^T(\mathbf{x}) = \begin{bmatrix} 1 & x & y & x^2 & xy & y^2 \end{bmatrix}.$$

All problems are resolved within the domain $\Omega = [0,1]^2$, and for the Gaussian weight function, we set $\mu = \frac{0.95}{\sqrt{M}-1}$. The support size is chosen to be $r = \frac{2.5}{\sqrt{M}-1}$ for all weight functions.

Example 1. Consider the first problem studied in [19] and [31]:

$$\begin{cases} \frac{\partial u}{\partial t} - \frac{\partial \Delta u}{\partial t} - \Delta u + \nabla \cdot u = \nabla \cdot G(u) + g(x,y,t), \\ (x,y) \in \Omega, \quad t \in (0,T], \\ u(x,y,0) = 0, \quad (x,y) \in \Omega, \\ u(x,y,t) = t\sin(x+y), \ (x,y) \in \partial\Omega, \text{ and } t \in [0,T]. \end{cases}$$

using the functions $G(u)$ and $g(x,y,t)$ as follows:

$$\begin{cases} G(u) & = \frac{u^2}{2}, \\ g(x,y,t) & = (3 + 2t - 2t^2 cos(x+y))sin(x+y) \\ & +2tcos(x+y) \end{cases}$$

and the exact solution is $u(x,y,t) = t\sin(x+y)$.

L_2 and L_∞ error norms are presented and compared with MCBSDQ and LSEM [19], [31] in table I. There is a clear and positive correlation observed between the outcomes obtained from the current method and those generated by the LSEM and MCBSDQ. The presentation of weight function comparisons and errors at $T = 1$ with various values of M and N are shown in tables II and III, where $N = 1280$ and $M = 625$, respectively. The precision and convergence of this approach can be observed through various weight functions, with the Gaussian weight function exhibiting higher accuracy than the others. Figure 1 plots the exact solution and associated approximate solution where $T = 1$ and $N = M = 100$. This numerical approximation is similar to the exact solution. The L_∞ error of the approximation in Figure 1 is presented in Figure 2 with numerous values of M, N, and T on the right side, and with $M = N = 100$ on the left side at $T = 1$. Consequently, it is clear that increasing values of N and M show convergence. The graphical representation shows that the spectral radius λ_{sr} of $\mathbf{W}$ systematically has magnitudes less than 1 in the two combinations in figure 3, this observation underlines the stability with different values of N, M and T. Moreover, we obtain that this stability is independent of space.

Example 2. Let us discuss the second problem as studied in [18], [31]:

$$\begin{cases} \frac{\partial u}{\partial t} - \frac{\partial \Delta u}{\partial t} - \Delta u + \nabla \cdot u = \nabla \cdot G(u) + g(x,y,t), \\ (x,y) \in \Omega, \quad t \in (0,T], \\ u(x,y,0) = exp(2x+2y), \quad (x,y) \in \Omega, \\ u(x,y,t) = exp(2x+2y+2t), \ (x,y) \in \partial\Omega, \ t \in [0,T], \end{cases}$$

where the functions $g(x,y,t)$ and $G(u)$ are given as follows:

$$\begin{cases} G(u) & = sin(u), \\ g(x,y,t) & = 2exp(2x+2y+2t) \\ & \times(9 + 2cos(exp(2x+2y+2t))) \end{cases}$$

and the exact solution is $u(x,y,t) = exp(2x+2y+2t)$.

The approximate numerical solution generated from the MLS method is shown in figure 4 with their exact solution at $T = 1$, $M = 625$ and $N = 80$. The numerical solution fit to the exact solution, demonstrating a high degree of accuracy. Additionally, the results of two methods reported in the articles [31], [18] with $T = 1$ and $M = 625$ are compared to the error L_∞ on various Δt for the MLS method in table IV. A remarkable agreement can be observed between the current method and those methods. Furthermore, the stability condition is validated for this Example 2 on different values of T in figure 5.

Example 3. Considering the problem (1) in this form:

$$\begin{cases} \frac{\partial u}{\partial t} - \frac{\partial \Delta u}{\partial t} - \Delta u + \nabla \cdot u = \nabla \cdot G(u) + g(x,y,t), \\ (x,y) \in \Omega, \quad t \in (0,T], \\ u(x,y,0) = (x-y+2)^\varphi, \quad (x,y) \in \Omega, \\ u(x,y,t) = \mathrm{e}^{t^2}(x-y+2)^\varphi, \ (x,y) \in \partial\Omega, \ t \in [0,T]. \end{cases} \tag{34}$$

Table I
Comparison of error norms and methods for Example 1 using GWF with $M = 400$ and $T = 1$.

	Proposed method		Method in [31]		Method in [19]	
Δt	L_2	L_∞	L_2	L_∞	L_2	L_∞
1/10	$2.1159e-02$	$2.0925e-03$	$2.3223e-02$	$2.1534e-03$	$3.2022e-02$	$2.0047e-03$
1/20	$1.0562e-02$	$1.0454e-03$	$1.2099e-02$	$1.1045e-03$	$1.6390e-02$	$1.0264e-03$
1/40	$5.2556e-03$	$5.2091e-04$	$6.5394e-03$	$5.7895e-04$	$8.2882e-03$	$5.1917e-04$
1/80	$2.6011e-03$	$2.5852e-04$	$3.7764e-03$	$3.1610e-04$	$4.1673e-03$	$2.6107e-04$
1/160	$1.2740e-03$	$1.2729e-04$	$2.4171e-03$	$1.8620e-04$	$2.0994e-03$	$1.3090e-04$
1/320	$6.1133e-04$	$6.1666e-05$	$1.7585e-03$	$1.2196e-04$	$1.0462e-03$	$6.5543e-05$
1/640	$2.8197e-04$	$2.8854e-05$	$1.4429e-03$	$9.2146e-05$	$5.2344e-04$	$3.2794e-05$
1/1280	$1.2262e-04$	$1.2888e-05$	$1.2915e-03$	$8.3407e-05$	$2.6181e-04$	$1.6403e-05$

Table II
L_∞-error, RMS-error and weight functions for Example 1 where $N = 1280$ and $T = 1$.

	The Gaussian weight		The Cubic spline weight		The Quartic spline weight	
M	L_∞-error	RMS-error	L_∞-error	RMS-error	L_∞-error	RMS-error
36	$6.7640e-04$	$2.3085e-04$	$9.6458e-04$	$3.8496e-04$	$1.3025e-03$	$5.7051e-04$
81	$1.7001e-04$	$4.8380e-05$	$4.1168e-04$	$1.8821e-04$	$5.5833e-04$	$2.7106e-04$
169	$5.0908e-05$	$1.1448e-05$	$2.2335e-04$	$1.0509e-04$	$2.8171e-04$	$1.4077e-04$
225	$3.2129e-05$	$7.2912e-06$	$1.7343e-04$	$8.3300e-05$	$2.1549e-04$	$1.0848e-04$
289	$2.1554e-05$	$6.1394e-06$	$1.3919e-04$	$6.7998e-05$	$1.7345e-04$	$8.6567e-05$

Table III
L_∞-error, RMS-error and weight functions for Example 1 where $M = 625$ and $T = 1$.

	The Gaussian weight		The Cubic spline weight		The Quartic spline weight	
N	L_∞-error	RMS-error	L_∞-error	RMS-error	L_∞-error	RMS-error
10	$2.0998e-03$	$1.0693e-03$	$2.1517e-03$	$1.0970e-03$	$2.1622e-03$	$1.1042e-03$
50	$4.1766e-04$	$2.1222e-04$	$4.7326e-04$	$2.4191e-04$	$4.8601e-04$	$2.5017e-04$
250	$8.0503e-05$	$4.0554e-05$	$1.3811e-04$	$7.1069e-05$	$1.5120e-04$	$7.9298e-05$
700	$2.6302e-05$	$1.3021e-05$	$8.5475e-05$	$4.3952e-05$	$9.8071e-05$	$5.1972e-05$
1000	$1.7285e-05$	$8.4721e-06$	$7.6886e-05$	$3.9489e-05$	$8.9263e-05$	$4.7437e-05$
1600	$1.0007e-05$	$4.5767e-06$	$6.9371e-05$	$3.5611e-05$	$8.1664e-05$	$4.3477e-05$

Table IV
Comparison of methods and L_∞ error for Example 2 using GWF with $M = 625$ and $T = 1$.

	Proposed method	Method in [31]	Method in [18]
Δt	L_∞	L_∞	L_∞
1/40	$4.2143e-02$	$7.6725e-02$	$5.3785e-01$
1/80	$1.8343e-02$	$7.3704e-02$	$2.8259e-01$
1/160	$1.8239e-02$	$7.2754e-02$	$1.4291e-01$
1/320	$1.8176e-02$	$7.1929e-02$	$7.2687e-01$

Whereas $g(x, y, t)$ and $G(u)$ are given as:

$$\begin{cases} G(u) &= cos(u)sin(u) \\ g(x,y,t) &= 2\,t\mathrm{e}^{t^2}\,(x-y+2)^{\varphi} - 4\,\frac{t\mathrm{e}^{t^2}\,(x-y+2)^{\varphi}(\varphi)^2}{(x-y+2)^2} \\ & +4\,\frac{t\mathrm{e}^{t^2}\,(x-y+2)^{\varphi}(\varphi)}{(x-y+2)^2} - 2\,\frac{\mathrm{e}^{t^2}\,(x-y+2)^{\varphi}(\varphi)^2}{(x-y+2)^2} \\ & +2\,\frac{\mathrm{e}^{t^2}\,(x-y+2)^{\varphi}(\varphi)}{(x-y+2)^2} \end{cases}$$

and the exact solution is $u(x, y, t) = \mathrm{e}^{t^2}\,(x - y + 2)^{\varphi}$ where $\varphi = \frac{1+\sqrt{5}}{2}$.

Table VI compare the weight functions and errors for varying values of M and N is presented at $T = 1$. Similarly, table VII performs a comparison of weight functions with $N = 500$ and $T = 1$ while varying M. These results validate the superiority of the GWF over the others in terms of exactness and efficiency. The different errors are displayed in table V for both $T = 1$ and $T = 2$, considering various combinations of M and N. The errors in table V are displayed for both $T = 1$ and $T = 2$, considering various numbers of M and N. Increasing the values of M and N clearly yields more accurate results when employing this method. Figure 6 exhibits the plots of the numerical and exact solutions when $M = 121$, $N = 100$ and $T = 1$. It is evident that the graphs demonstrate the same thing. Figure 7 illustrates the verification of the stability of the current method. The magnitudes of the eigenvalues of matrix $\mathbf{W}$ are depicted in figure 7 with $T = 3$ and $T = 1$ for different numbers of M and N, respectively. As shown in this figure the magnitudes of the eigenvalues remain below 1 for Example 3.

Example 4. The second test problem (1) is considered as:

$$\begin{cases} \frac{\partial u}{\partial t} - \frac{\partial \Delta u}{\partial t} - \Delta u + \nabla \cdot u = \nabla \cdot G(u) + g(x,y,t), \\ (x,y) \in \Omega, \quad t \in (0,T], \\ u(x,y,0) = cosh(x+y), \quad (x,y) \in \Omega, \\ u(x,y,t) = sinh(t)cosh(x+y), \; (x,y) \in \partial\Omega, \\ \text{and } t \in [0,T], \end{cases}$$

with the known function $g(x, y, t)$ and the nonlinear term

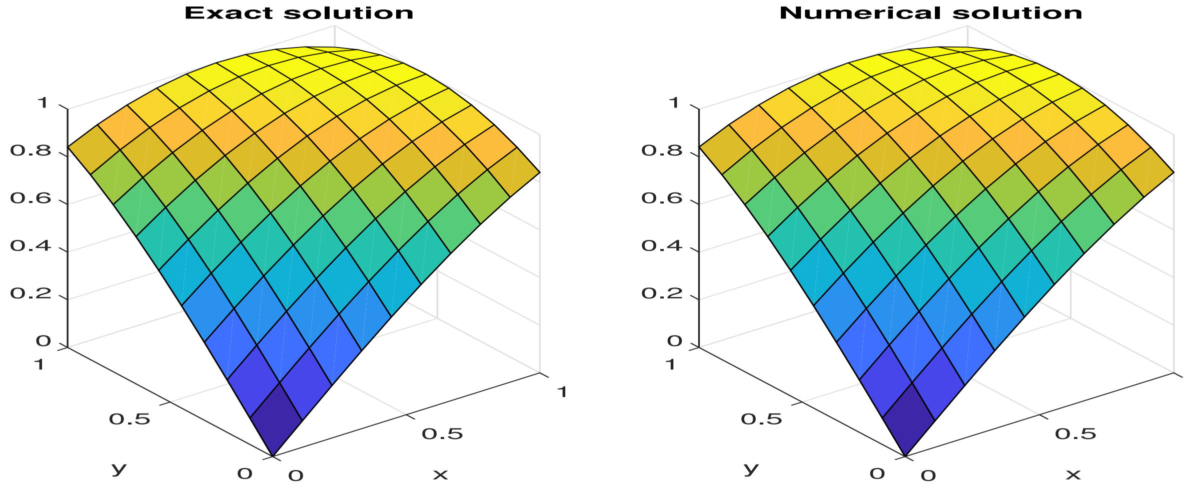

Figure 1. The graphs for Example 1 where $M = N = 100$ and $T = 1$.

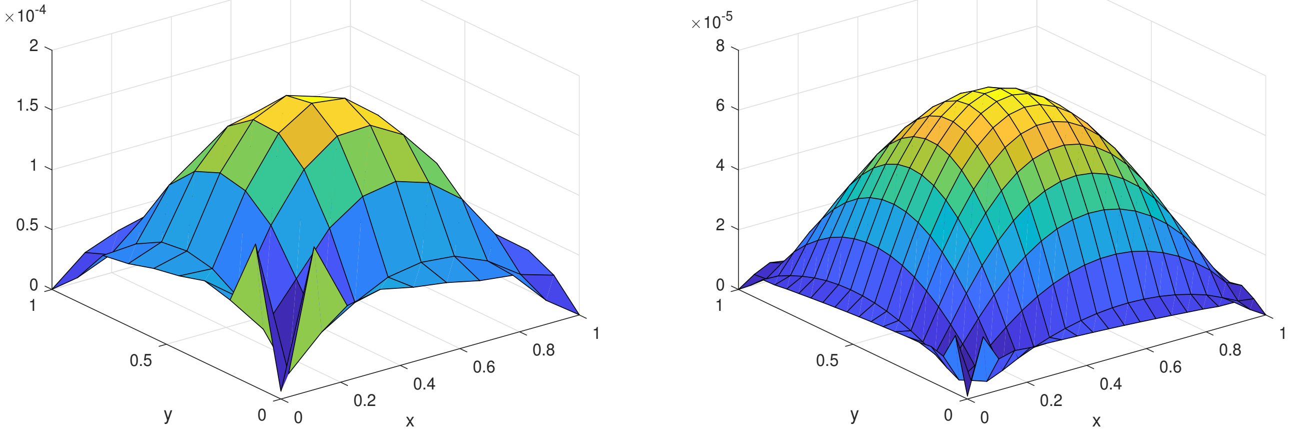

Figure 2. The L_∞ error using GWF for Example 1 at $M = N = 100$ and $T = 1$ (left) and at $T = 1.5$ where $M = 400$ and $N = 800$ (right).

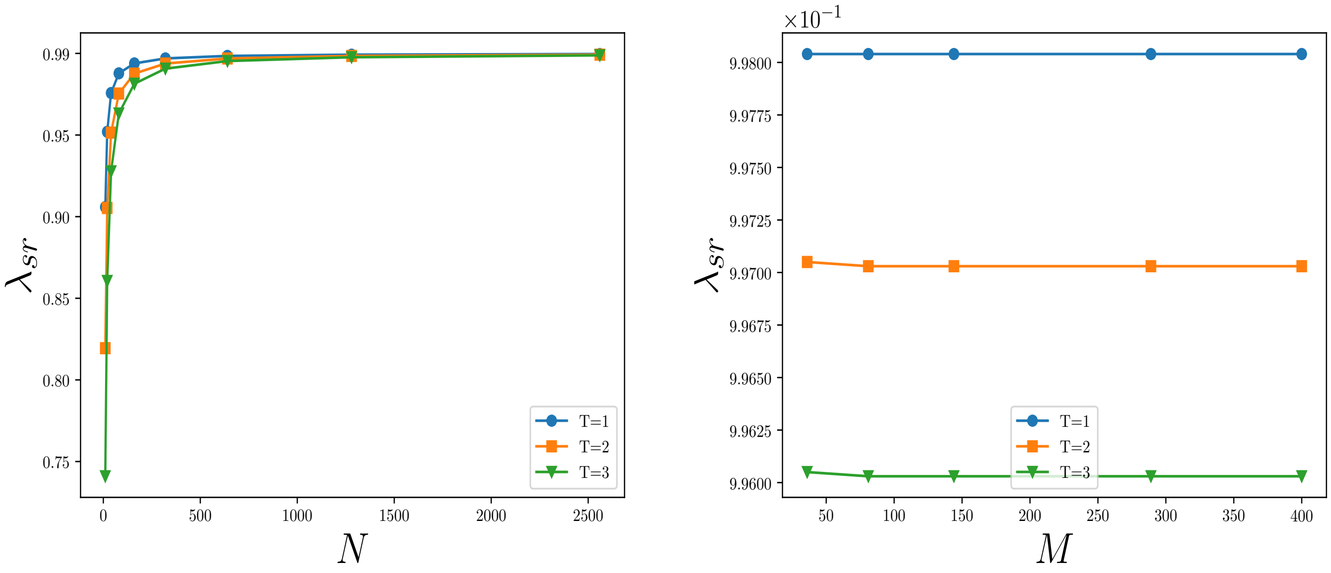

Figure 3. The magnitude of $\mathbf{W}$ matrix's for Example 1 where $M = 625$ (left panel) and $N = 1280$ (right panel) with various value of M, N and T, respectively.

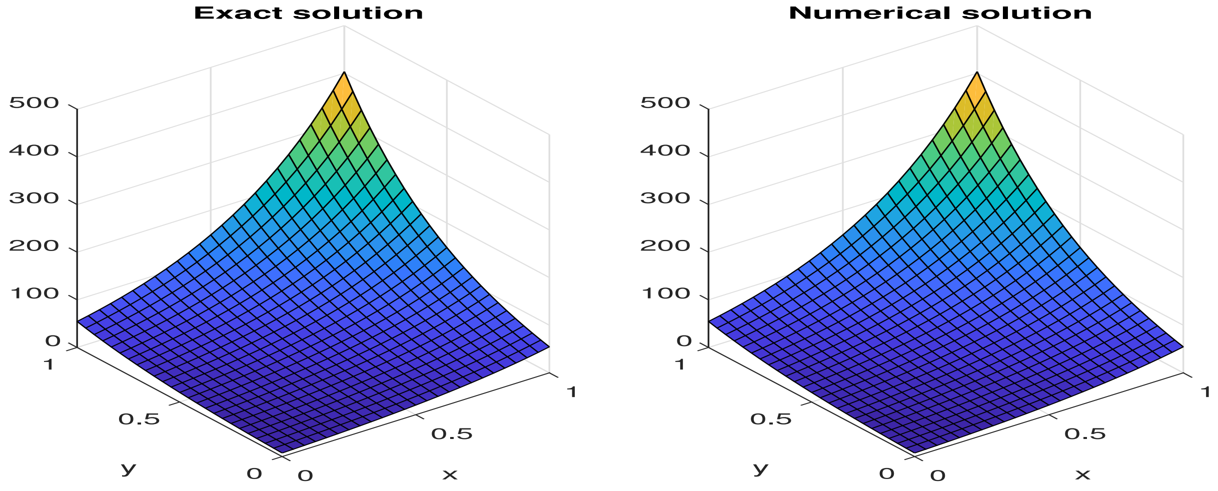

Figure 4. The graphs for Example 2 where $T = 1$, $M = 625$ and $N = 80$.

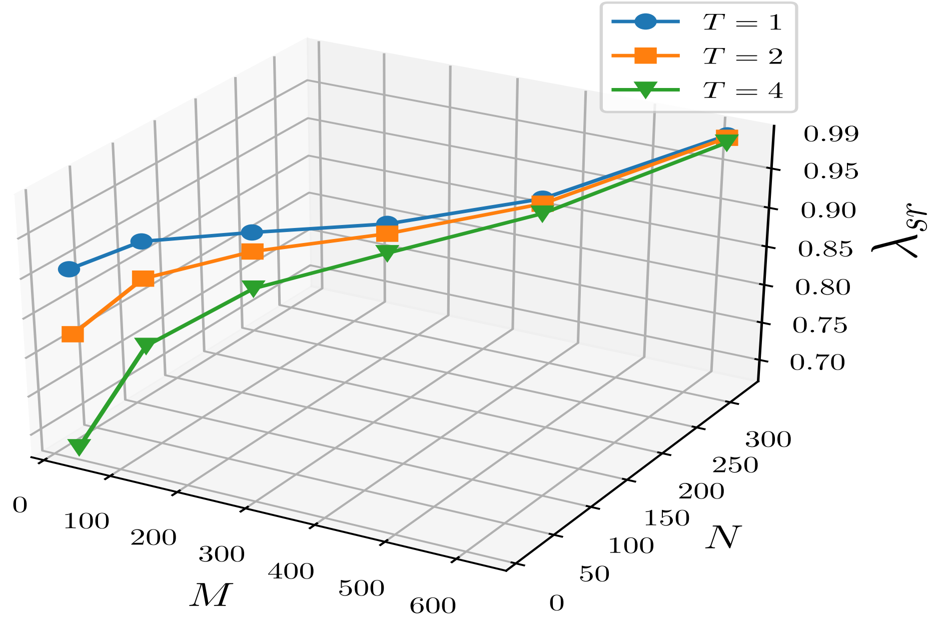

Figure 5. The λ_{sr} of $\mathbf{W}$ matrix's where varying values of T for Example 2.

$G(u)$ as:

$$G(u) = tanh(u),$$
$$g(x,y,t) = -\cosh(t)\cosh(x+y) - 2\sinh(t)\cosh(x+y)$$
$$+ 2\sinh(t)\sinh(x+y) - 2\sinh(t)\sinh(x+y)$$
$$\times \left(1 - (\tanh(\sinh(t)\cosh(x+y)))^2\right)$$

and the exact solution is $u(x,y,t) = sinh(t)cosh(x+y)$.

With different combinations of N and M, the errors are illustrated in the table $VIII$ for both $T = 1$ and $T = 2$. We can see the convergence of the present technique as the values of N and M increase. The error comparisons presented in table IX focused on $T = 0.5$ and $T = 1$ with a fixed value of $M = 676$ while varying N. The same result of the Gaussian weight function is very accurate. Similarly, the error comparisons provided in table X concentrate on $T = 0.5$ and $T = 1$, with $N = 1000$ while varying M. Indeed, the results in tables $VIII$, IX and X confirm of the convergence and exactness of this technique when increasing the values of M and N, respectively. In Figure 9, we present the solutions with $M = 400$, $N = 100$, and $T = 0.5$ for Example 4. The graph shows that the approximate and exact solutions are the same. The L_∞ error of the above graph is illustrated in figure 8, considering $M = 400$, $N = 100$ and $T = 0.5$. In figure 10, the magnitudes of

Table V
The L_∞, L_2 and RMS errors for Example 3 using GWF.

		$T=1$			$T=2$		
N	M	L_∞-error	L_2-error	RMS-error	L_∞-error	L_2-error	RMS-error
40	36	$5.1679e-04$	$1.0071e-03$	$1.6786e-04$	$2.0504e-02$	$5.8742e-02$	$9.7904e-03$
70	49	$3.1432e-04$	$6.3638e-04$	$9.0912e-05$	$6.6829e-03$	$2.6224e-02$	$3.7462e-03$
120	100	$1.0196e-04$	$2.4286e-04$	$2.4286e-05$	$2.3105e-03$	$1.2570e-02$	$1.2570e-03$
200	169	$4.5128e-05$	$1.2137e-04$	$9.3363e-06$	$9.1317e-04$	$6.1200e-03$	$4.7077e-04$
300	256	$2.3799e-05$	$6.9569e-05$	$4.3481e-06$	$4.8168e-04$	$3.3377e-03$	$2.0860e-04$
480	361	$1.4072e-05$	$5.6234e-05$	$2.9597e-06$	$2.8503e-04$	$2.2394e-03$	$1.1787e-04$

Table VI
The L_∞, RMS errors and weight functions for Example 3 where $T=1$.

		The Gaussian weight		The Cubic spline weight		The Quartic spline weight	
N	M	L_∞-error	RMS-error	L_∞-error	RMS-error	L_∞-error	RMS-error
15	9	$3.7942e-03$	$2.1460e-03$	$5.4161e-03$	$2.9984e-03$	$6.9197e-03$	$3.7782e-03$
50	25	$9.3167e-04$	$3.2907e-04$	$1.3070e-03$	$4.6899e-04$	$1.7398e-03$	$5.8854e-04$
100	49	$3.1434e-04$	$8.9712e-05$	$4.4347e-04$	$1.4592e-04$	$5.9629e-04$	$1.9383e-04$
200	121	$7.5752e-05$	$1.6806e-05$	$1.0697e-04$	$4.5751e-05$	$1.4427e-04$	$6.4616e-05$
300	196	$3.5897e-05$	$7.0782e-06$	$5.2749e-05$	$2.7961e-05$	$8.1806e-05$	$3.8864e-05$
500	361	$1.4072e-05$	$2.9488e-06$	$2.9985e-05$	$1.5701e-05$	$5.5329e-05$	$2.2285e-05$

Table VII
The weight functions, L_∞-error and RMS-error for Example 3 where $N=500$ and $T=1$.

	The Gaussian weight		The Cubic spline weight		The Quartic spline weight	
M	L_∞-error	RMS-error	L_∞-error	RMS-error	L_∞-error	RMS-error
16	$2.0212e-03$	$8.2348e-04$	$2.8353e-03$	$1.1982e-03$	$3.7825e-03$	$1.5265e-03$
36	$5.1683e-04$	$1.6080e-04$	$7.3053e-04$	$2.4686e-04$	$9.8784e-04$	$3.2500e-04$
64	$2.0565e-04$	$5.3717e-05$	$2.9043e-04$	$1.0106e-04$	$3.9244e-04$	$1.3858e-04$
144	$5.7819e-05$	$1.2122e-05$	$8.1655e-05$	$3.8794e-05$	$1.1458e-04$	$5.4356e-05$
324	$1.6575e-05$	$3.0929e-06$	$3.3924e-05$	$1.7983e-05$	$5.4608e-05$	$2.4010e-05$

Table VIII
The L_∞, L_2 and RMS errors for Example 4 using GWF.

		$T=1$			$T=2$		
N	M	L_∞-error	L_2-error	RMS-error	L_∞-error	L_2-error	RMS-error
80	25	$4.0010e-03$	$6.6343e-03$	$1.3269e-03$	$1.2326e-02$	$2.0186e-02$	$4.0372e-03$
180	49	$1.3546e-03$	$2.5631e-03$	$3.6615e-04$	$4.1758e-03$	$7.7523e-03$	$1.1075e-03$
400	100	$4.3710e-04$	$9.7794e-04$	$9.7794e-05$	$1.3480e-03$	$2.9250e-03$	$2.9250e-04$
600	144	$2.4693e-04$	$6.0742e-04$	$5.0619e-05$	$7.6161e-04$	$1.8030e-03$	$1.5025e-04$
1000	676	$2.9430e-05$	$1.7041e-04$	$6.5543e-06$	$8.9412e-05$	$4.8303e-04$	$1.8578e-05$

Table IX
The L_∞, L_2 and RMS errors for Example 4 using GWF where $M=676$.

	$T=0.5$			$T=1$		
N	L_∞-error	L_2-error	RMS-error	L_∞-error	L_2-error	RMS-error
50	$1.5829e-04$	$2.1524e-03$	$8.2786e-05$	$6.2892e-05$	$5.4092e-04$	$2.0805e-05$
150	$5.2230e-05$	$7.0390e-04$	$2.7073e-05$	$3.5462e-05$	$2.6894e-04$	$1.0344e-05$
300	$2.5906e-05$	$3.4575e-04$	$1.3298e-05$	$3.0241e-05$	$2.0694e-04$	$7.9592e-06$
600	$1.2763e-05$	$1.7279e-04$	$6.6459e-06$	$2.9662e-05$	$1.7995e-04$	$6.9212e-06$
900	$1.2595e-05$	$1.2042e-04$	$4.6315e-06$	$2.9469e-05$	$1.7194e-04$	$6.6132e-06$

Table X
The L_∞, L_2 and RMS errors for Example 4 using GWF with $N=1000$.

	$T=0.5$			$T=1$		
M	L_∞-error	L_2-error	RMS-error	L_∞-error	L_2-error	RMS-error
36	$9.8835e-04$	$1.7766e-03$	$2.9611e-04$	$2.2262e-03$	$3.9430e-03$	$6.5717e-04$
144	$1.0953e-04$	$2.6535e-04$	$2.2113e-05$	$2.4692e-04$	$6.0450e-04$	$5.0375e-05$
324	$3.1210e-05$	$1.0065e-04$	$5.5917e-06$	$7.0374e-05$	$2.2042e-04$	$1.2246e-05$
576	$1.4379e-05$	$9.7581e-05$	$4.0659e-06$	$3.3451e-05$	$1.6856e-04$	$7.0234e-06$

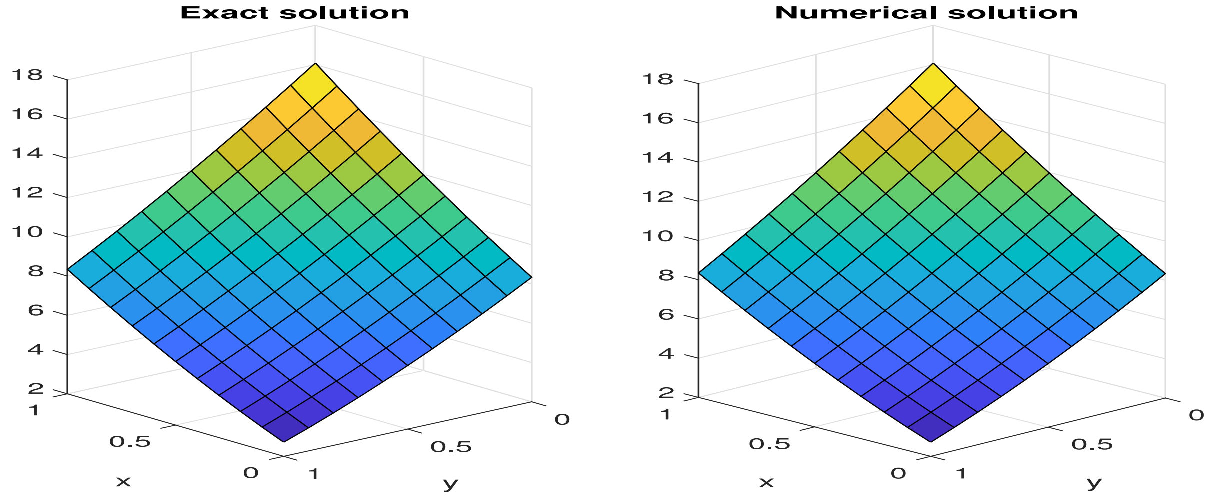

Figure 6. The graphs for Example 3 with $M = 121$, $N = 100$ and $T = 1$.

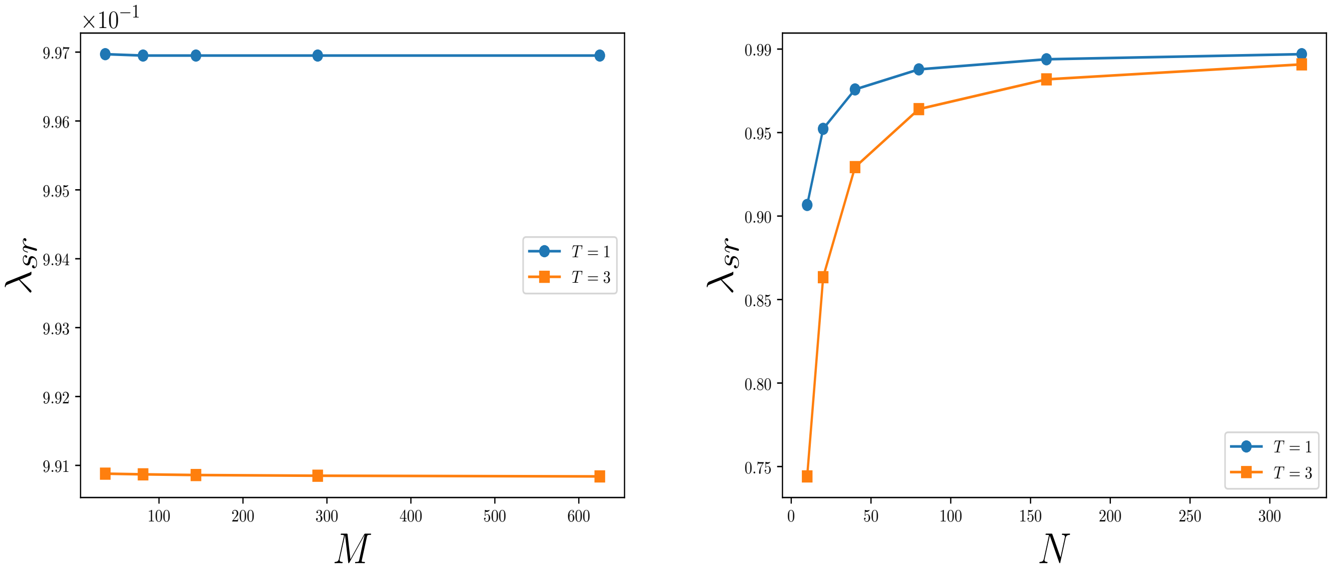

Figure 7. The magnitude of $\mathbf{W}$ matrix's for Example 3 where $M = 625$ (left panel) and $N = 320$ (right panel) with various value of M, N and T, respectively.

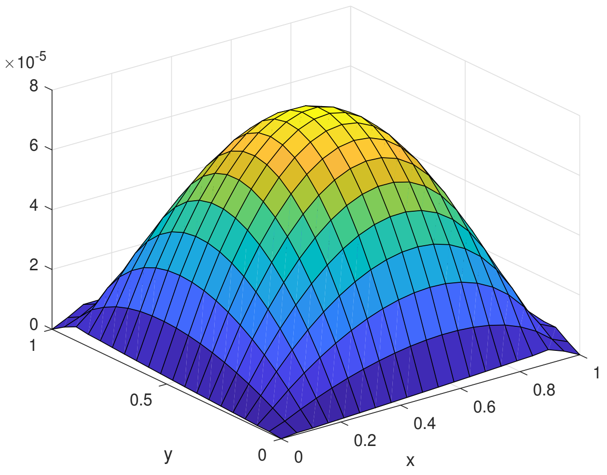

Figure 8. L_∞ error for Example 4 with $M = 400$, $N = 100$ and $T = 0.5$.

the eigenvalues of the $\mathbf{W}$ matrix are graphed for various combinations of T, with M and N as variables. The magnitudes of these eigenvalues consistently stay below 1, as demonstrated by figure 10. This confirms that the current approach for Example 4 is stable.

VI. Conclusion

In this article, we solve the generalized 2-D nonlinear BBMB equation using moving least squares. A FDM was employed for discretizing the time variable, aiming to find a semi-discrete scheme in the time direction. The validity of convergence and stability of the current method provided by numerical cases. The MLS method displays greater accuracy when compared to the meshless method of RBFs, and it also agrees well with the MCBSDQ and LSEM. The numerical findings underscore the remarkable similarity with the theoretical stability condition, making it versatile for use across various time intervals. This technique can be extended in the future

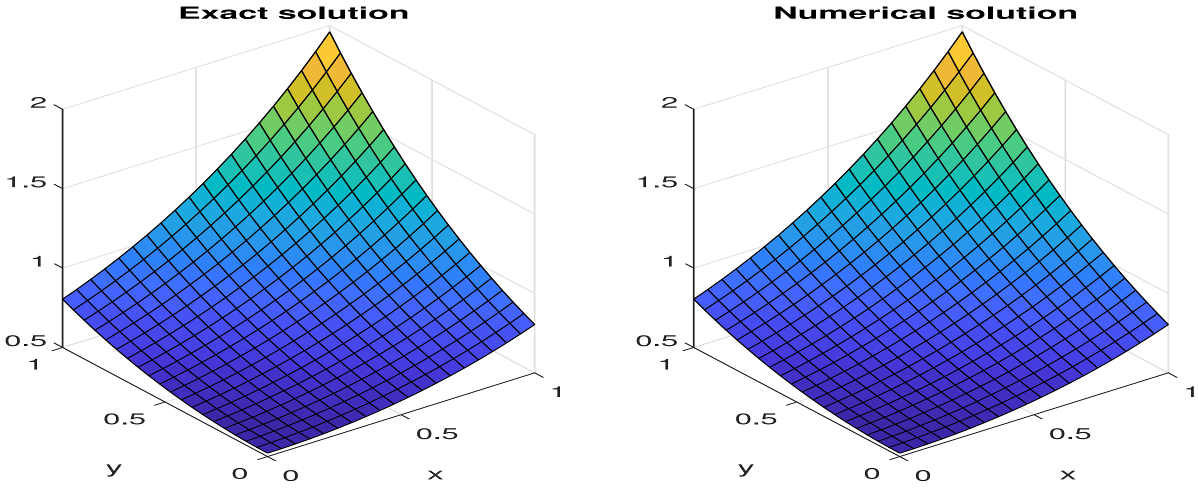

Figure 9. The graphs for Example 4 at $T = 0.5$ with $N = 100$ and $M = 400$.

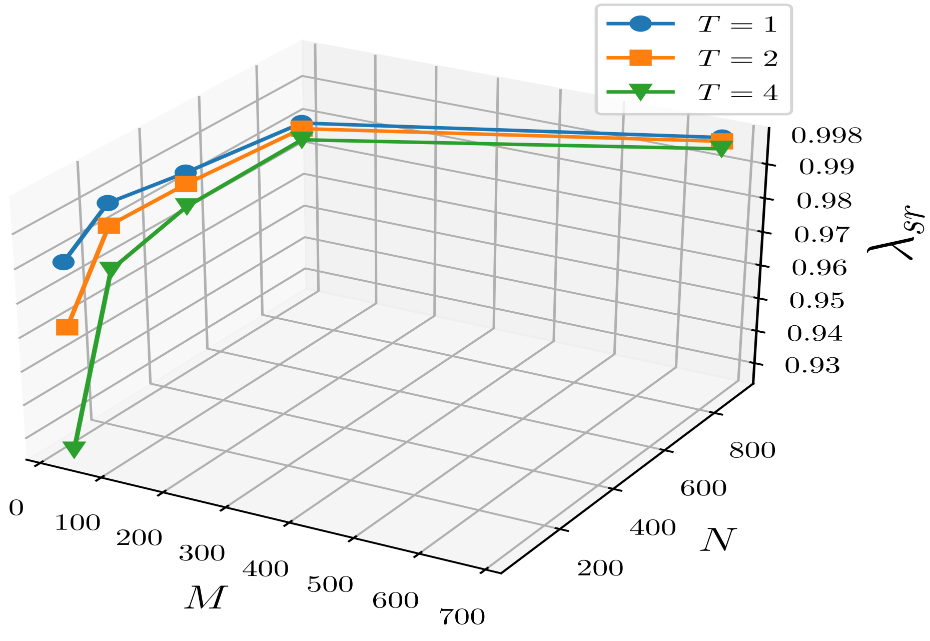

Figure 10. The λ_{sr} of $\mathbf{W}$ matrix's with three values of T for Example 4.

to address associated problems and other situations of fractional partial differential equations (FPDEs) in regular and irregular domains $\Omega \subset \mathbb{R}^d$ $(d \geq 2)$.

References

[1] S. Abbasbandy and A. Shirzadi. The first integral method for modified benjamin–bona–mahony equation. Communications in Nonlinear Science and Numerical Simulation, 15(7):1759–1764, 2010.

[2] M. Abdollahzadeh, M. Ghanbarpour, A. Hosseini, and S. Kashani. Exact travelling solutions for benjamin-bona-mahony-burgers equations by (g'/g)-expansion method. International Journal of Applied Mathematics and Computation, 3(1):70–76, 2010.

[3] T. Achouri and K. Omrani. Application of the homotopy perturbation method to the modified regularized long-wave equation. Numerical Methods for Partial Differential Equations: An International Journal, 26(2):399–411, 2010.

[4] O. Adeyemo, C. Khalique, Y. Gasimov, and F. Villecco. Variational and non-variational approaches with lie algebra of a generalized (3 + 1)-dimensional nonlinear potential yu-toda-sasa-fukuyama equation in engineering and physics. Alexandria Engineering Journal, 63, 09 2022.

[5] U. Akram, A. R. Seadawy, S. Rizvi, M. Younis, S. Althobaiti, and S. Sayed. Traveling wave solutions for the fractional wazwaz–benjamin–bona–mahony model in arising shallow water waves. Results in Physics, 20:103725, 2021.

[6] S. Arora, R. Jain, and V. Kukreja. Solution of benjamin-bona-mahony-burgers equation using collocation method with quintic hermite splines. Applied Numerical Mathematics, 154:1–16, 2020.

[7] M. Aslefallah, S. Abbasbandy, and E. Shivanian. Meshless formulation to two-dimensional nonlinear problem of generalized benjamin–bona–mahony–burgers through singular boundary

method: Analysis of stability and convergence. Numerical Methods for Partial Differential Equations, 36(2):249–267, 2020.

[8] T. Belytschko, Y. Y. Lu, and L. Gu. Element-free galerkin methods. International Journal for Numerical Methods in Engineering, 37(2):229–256, 1994.

[9] T. Benjamin, J. Bona, and J. Mahony. Model equations for long waves in nonlinear dispersive systems. Philosophical Transactions of The Royal Society B: Biological Sciences, 272:47–78, 03 1972.

[10] J. Biazar and S. Safaei. An analytic approximation for time-fractional bbm-burger equation. Punjab University Journal of Mathematics, 52(8), 2020.

[11] R. B. Bird. Nonlinear partial differential equations in engineering, w. f. ames, academic press, new york (1965). 511 pages + xii. 50 figures in the text. AIChE Journal, 12(2):410–412, 1966.

[12] J. L. Bona and P. J. Bryant. A mathematical model for long waves generated by wavemakers in non-linear dispersive systems. Mathematical Proceedings of the Cambridge Philosophical Society, 73(2):391–405, 1973.

[13] H. Brezis. Functional Analysis, Sobolev Spaces and Partial Differential Equations. Universitext. Springer New York, 2010.

[14] M. S. Bruzón, T. M. Garrido-Letrán, and R. de la Rosa. Symmetry analysis, exact solutions and conservation laws of a benjamin–bona–mahony–burgers equation in 2+ 1-dimensions. Symmetry, 13(11):2083, 2021.

[15] M. S. Bruzón, T. M. Garrido-Letrán, and R. de la Rosa. Symmetry analysis, exact solutions and conservation laws of a benjamin–bona–mahony–burgers equation in 2+1-dimensions. Symmetry, 13(11), 2021.

[16] M. Darvishi and M. Najafi. Exact three-wave solutions for high nonlinear form of benjamin-bona-mahony-burgers equations. World Academy of Science, Engineering and Technology, 37:489–493, 01 2010.

[17] L. Debnath. Nonlinear Partial Differential Equations for Scientists and Engineers. Birkhäuser Boston, 2011.

[18] M. Dehghan, M. Abbaszadeh, and A. Mohebbi. The numerical solution of nonlinear high dimensional generalized benjamin–bona–mahony–burgers equation via the meshless method of radial basis functions. Computers & Mathematics with Applications, 68, 08 2014.

[19] M. Dehghan, N. Shafieeabyaneh, and M. Abbaszadeh. Numerical and theoretical discussions for solving nonlinear generalized benjamin–bona–mahony–burgers equation based on the legendre spectral element method. Numerical Methods for Partial Differential Equations, 10 2020.

[20] B.-Q. Dong, C. Zhao, X. Qin, L. Zhang, L. Li, et al. Nonlinear partial differential equations in mathematics and physics. In Abstract and Applied Analysis, volume 2015. Hindawi, 2015.

[21] Z. El Majouti, E. Taghizadeh, and R. El Jid. A meshless method for the numerical solution of fractional stochastic integro-differential equations based on the moving least square approach. International Journal of Applied and Computational Mathematics, 9(3):27, 2023.

[22] J. Flores, A. García, M. Negreanu, E. Salete, F. Ureña, and A. Vargas. A spatio-temporal fully meshless method for hyperbolic pdes. Journal of Computational and Applied Mathematics, 430:115194, 2023.

[23] R. Franke and G. Nielson. Smooth interpolation of large sets of scattered data. International Journal for Numerical Methods in Engineering, 15(11):1691–1704, 1980.

[24] T. P. Fries and H. G. Matthies. Classification and overview of meshfree methods. 2004.

[25] Z. Ganji, D. Ganji, and H. Bararnia. Approximate general and explicit solutions of nonlinear bbmb equations by exp-function method. Applied Mathematical Modelling, 33(4):1836–1841, 2009.

[26] H. Hajinezhad and A. R. Soheili. A numerical approximation for the solution of a time-fractional telegraph equation by the moving least squares approach. Computational Methods for Differential Equations, 2023.

[27] S. Haq, A. Ghafoor, M. Hussain, and S. Arifeen. Numerical solutions of two dimensional sobolev and generalized benjamin–bona–mahony–burgers equations via haar wavelets. Computers & Mathematics with Applications, 77(2):565–575, 2019.

[28] B. Hong and D. Lu. New exact solutions for the generalized bbm and burgers-bbm equations. ISSN UK World Journal of Modelling and Simulation, 1:746–7233, 01 2008.

[29] M. Hosseininia and M. Heydari. Meshfree moving least squares method for nonlinear variable-order time fractional 2d telegraph equation involving mittag–leffler non-singular kernel. Chaos, Solitons & Fractals, 127:389–399, 2019.

[30] M. Hosseininia, M. Heydari, F. M. Ghaini, and Z. Avazzadeh. A meshless technique based on the moving least squares shape functions for nonlinear fractal-fractional advection-diffusion equation. Engineering Analysis with Boundary Elements, 127:8–17, 2021.

[31] P. Joshi, M. Pathak, and J. Lin. Numerical study of generalized 2-d nonlinear benjamin–bona–mahony–burgers equation using modified cubic b-spline differential quadrature method. Alexandria Engineering Journal, 67:409–424, 03 2023.

[32] T. Kadri, N. Khiari, F. Abidi, and K. Omrani. Methods for the numerical solution of the benjamin-bona-mahony-burgers equation. Numerical Methods for Partial Differential Equations, 24(6):1501–1516, 2008.

[33] M. Kazeminia, P. Tolou, J. Mahmoudi, I. Khatami, and N. Tolou. Solitary and periodic solutions of bbmb equation via exp-function method. Advanced Studies in Theoretical Physics, 3(12):461–471, 2009.

[34] B. Kopçasız and E. YAŞAR. μ-symmetries and μ-conservation laws for the nonlinear dispersive modified benjamin-bona-mahony equation. Journal of Mathematical Sciences and Modelling, pages 87–96, 07 2023.

[35] M. O. Korpusov and D. K. Yablochkin. Potential theory for a nonlinear equation of the benjamin–bona–mahoney–burgers type. Computational Mathematics and Mathematical Physics, 59:1848–1880, 2019.

[36] V. Kukreja et al. Numerical treatment of benjamin-bona-mahony-burgers equation with fourth-order improvised b-spline collocation method. Journal of Ocean Engineering and Science, 7(2):99–111, 2022.

[37] L.-X. Li and Z.-D. Dai. Degeneration of solitons for a (2+1)-dimensional bbmb equation in nonlinear dispersive media. Nonlinear Dynamics, 109, 05 2022.

[38] H. Mafikandi and M. Amirfakhrian. Solving linear partial differential equations by moving least squares method. differential equations, 3:4, 2015.

[39] Z. Mahboob Dana, H. S. Najafi, and A. Refahi Sheikhani. An efficient numerical method for solving benjamin–bona–mahony–burgers equation using difference scheme. Journal of difference equations and applications, 26(4):574–585, 2020.

[40] A. Majeed, M. Kamran, M. Abbas, and M. Y. B. Misro. An efficient numerical scheme for the simulation of time-fractional nonhomogeneous benjamin-bona-mahony-burger model. Physica Scripta, 96(8):084002, may 2021.

[41] A. Majeed, M. Kamran, M. Abbas, and M. Y. B. Misro. An efficient numerical scheme for the simulation of time-fractional nonhomogeneous benjamin-bona-mahony-burger model. Physica Scripta, 96(8):084002, 2021.

[42] A. Majeed, M. Kamran, M. Abbas, and M. Y. B. Misro. An efficient numerical scheme for the simulation of time-fractional nonhomogeneous benjamin-bona-mahony-burger model. Physica Scripta, 96(8):084002, 2021.

[43] A. Mardani, M. Hooshmandasl, M. Hosseini, and M. Heydari. Moving least squares (mls) method for the nonlinear hyperbolic telegraph equation with variable coefficients. International Journal of Computational Methods, 14(03):1750026, 2017.

[44] S. Mazumder. Numerical Methods for Partial Differential Equations: Finite Difference and Finite Volume Methods. Elsevier Science, 2015.

[45] B. Sagar and S. Saha Ray. Numerical and analytical investigation for solutions of fractional oskolkov–benjamin–bona–mahony–burgers equation describing propagation of long surface waves. International Journal of Modern Physics B, 35(32):2150326, 2021.

[46] D. Shepard. A two-dimensional interpolation function for irregularly-spaced data. In Proceedings of the 1968 23rd ACM national conference, pages 517–524, 1968.

[47] E. Shivanian. Meshless local petrov–galerkin (mlpg) method for three-dimensional nonlinear wave equations via moving least squares approximation. Engineering Analysis with Boundary Elements, 50:249–257, 2015.

[48] E. Shivanian and A. Jafarabadi. More accurate results for nonlinear generalized benjamin-bona-mahony-burgers (gbbmb) problem through spectral meshless radial point interpolation (smrpi). Engineering Analysis with Boundary Elements, 72:42–54, 2016.

[49] R. Sternberg, A. Kalinowski, and J. Papadakis. Nonlinear Partial Differential Equations in Engineering and Applied Science. Lecture Notes in Pure and Applied Mathematics. Taylor & Francis, 1980.

[50] K. Tariq, M. Inc, and M. Hashemi. Dynamic behavior of time-fractional benjamin-bona-mahony-burger model in fluids. 02 2023.

[51] A. Tayebi, Y. Shekari, and M. H. Heydari. A meshless method for solving two-dimensional variable-order time fractional advection–diffusion equation. Journal of computational physics, 340:655–669, 2017.

[52] J. Wan and X. Li. Analysis of a superconvergent recursive moving least squares approximation. Applied Mathematics Letters, 133:108223, 2022.

[53] B. Wang, D. W. Fussner, and C. Bi. Existence of global attractors for the benjamin–bona–mahony equation in unbounded domains. Journal of Physics A: Mathematical and Theoretical, 40(34):10491, aug 2007.

[54] Y.-X. Yin and G.-R. Piao. Quadratic b-spline finite element method for the benjamin-bona-mahony-burgers equation. East Asian mathematical journal, 29(5):503–510, 2013.

[55] Q. Zhang, L. Liu, and J. Zhang. The numerical analysis of two linearized difference schemes for the benjamin–bona–mahony–burgers equation. Numerical Methods for Partial Differential Equations, 36(6):1790–1810, 2020.

[56] H. Zhao and R. Admas. Existence and convergence of solutions for the generalized bbm-burgers equations with dissipative term 2: the multidimensional case. Applicable Analysis, 75:107–135, 06 2000.

[57] Y.-H. Zhao, T. Mathanaranjan, H. Rezazadeh, L. Akinyemi, and M. Inc. New solitary wave solutions and stability analysis for the generalized (3+1)-dimensional nonlinear wave equation in liquid with gas bubbles. Results in Physics, 43:106083, 2022.